Appl. Phys. A 83, 411–415 (2006)
DOI: 10.1007/s00339-006-3520-5

**Applied Physics A**
**Materials Science & Processing**

J. XU✉
J.S. THAKUR
G. HU
Q. WANG
Y. DANYLYUK
H. YING
G.W. AUNER

# Angular dependence of surface acoustic wave characteristics in AlN thin films on *a*-plane sapphire substrates

Department of Electrical and Computer Engineering, Wayne State University, Detroit, Michigan 48202, USA

**Received: 29 August 2005/Accepted: 9 January 2006**
**Published online: 1 March 2006 •** 

**ABSTRACT** AlN thin films have been grown on *a*-plane sapphire ($Al_2O_3(11\bar{2}0)$) substrates. X-ray diffraction measurements indicate the films are fully *c*-plane (0001) oriented with a full width at half maximum of the AlN(0002) rocking curves of 0.76–0.92°. The epitaxial growth relationships have been determined by the reflection high energy electron diffraction analysis as $AlN[1\bar{1}00]//Al_2O_3[0001]$ and $AlN[11\bar{2}0]//Al_2O_3[1\bar{1}00]$. Angular dependence of important surface acoustic wave (SAW) characteristics, such as the phase velocity and electromechanical coupling coefficient, has been investigated on the $AlN(0001)/Al_2O_3(11\bar{2}0)$ structure. While the SAW is excited at all propagation angles with an angular dispersion of the phase velocity in the range of 5503–6045 m/s, a higher velocity shear-horizontal (SH) mode is observed only at 0°, 105° and 180° off the reference $Al_2O_3[1\bar{1}00]$ over a 180° angular period. The phase velocity of the SH mode shows dispersion (6089–6132 m/s) as a function of the SAW wavelength. Temperature coefficients of frequency are also demonstrated for both modes.

**PACS** 81.15.Hi; 77.84.-s; 77.65.Dq

## 1 Introduction

AlN is a III–V semiconductor that has drawn widespread attention in the area of optical, high power and high temperature electronic devices. Its piezoelectricity and high SAW velocity, ∼ 5700 m/s [1, 2], makes it promising for miniaturized sensors applications as well as high frequency SAW devices in mobile communication systems. The resonance frequency of a SAW device is given as $f_0 = \nu_p/\lambda$, where $\nu_p$ denotes the phase velocity and $\lambda$ the wavelength. The trend towards high frequency SAW devices in communications could be satisfied by either employing a material with large $\nu_p$ or by the reduction of $\lambda$ that is defined by the periodicity of interdigital transducers (IDTs). However, the latter becomes resource extensive beyond a certain process limit. On the other hand, high sensitivity is always desirable for SAW sensors, especially in the fast growing biological and chemical sensing fields. Underlying numerous SAW sensor applications, mass loading is the predominant sensing mechanism [3, 4], which states that the fractional change in resonance frequency or phase velocity of the SAW is the negative of the fractional change in device surface mass density ($\varrho$): $\Delta f/f_0 = \Delta\nu_p/\nu_p = -\Delta\varrho/\varrho$. As a result, a high SAW velocity material like AlN would lead to a high mass sensitivity for the fact that a relative small change in surface mass would induce a large detectable frequency shift [5].

Besides the aforementioned advantages, by incorporating physical properties of the substrate material, the layered structure of AlN offers flexible control over the phase velocity, electromechanical coupling coefficient ($K^2$), and temperature coefficient of frequency (TCF) [6–8]. The interaction between the film and substrate may also give rise to new acoustic modes other than the ordinary Rayleigh SAW with proper boundary conditions. For instance, Love waves could appear when the overlayer has a slower shear velocity than that of the substrate and Pseudo-SAWs (PSAWs) or their degenerated quasibulk counterpart like surface skimming bulk waves are observed in anisotropic film/substrate combinations with strong angular dependence [9–12]. These waves usually travel at a higher velocity than the 1st order SAW mode. They may possess other distinct features such as SH polarization resulting from the contribution of the quasi-shear bulk partial wave [9]. Such SH polarization is especially useful in aqueous biosensing applications, in which conventional SAW sensors suffer excessive energy loss due to energy dissipation into surrounding fluid in the form of a compressional wave [3]. Therefore, it would be of practical importance to investigate the effect of the substrate orientation and wave propagation angles on the SAW characteristics in AlN thin films.

AlN thin films are most commonly grown on sapphire substrate for good expitaxial growth and affordable price. Most of the work regarding SAWs in AlN thin films on sapphire substrates focused on the $AlN(0001)/Al_2O_3(0001)$ or $AlN(11\bar{2}0)/Al_2O_3(1\bar{1}02)$ structure [2, 13, 14]. In this work, we report the growth of epitaxial AlN(0001) on $Al_2O_3(11\bar{2}0)$ substrates and the study of SAW characteristics under the presence of an anisotropic $Al_2O_3(11\bar{2}0)$ substrate. The focus herein is two-fold: first, the effect of propagation angle on the SAW characteristics; second, the excitation of the SH mode at isolated propagation angles.

✉ Fax: +1-313-577-1101, E-mail: jianzeng@ece.eng.wayne.edu

## 2 Experimental

AlN thin films were grown on $Al_2O_3(11\bar{2}0)$ by a method of plasma source molecular beam epitaxy [15]. The base vacuum of the system was at the level of $10^{-9}$ Torr. The growth temperature was set at 650 °C. $N_2$ and Ar gases were delivered into the chamber at a rate of 10 sccm and 40 sccm, respectively. The generated plasma was maintained by a power of 200 W at 13.56 MHz. The film thicknesses measured by a profilometer are in the range of 1.4 to 2.2 μm. The growth orientations and crystalline quality were evaluated by a X-ray diffraction (XRD) system using Cu $K_\alpha$ radiation sources ($\lambda = 1.54178$ Å) and a reflection high energy electron diffraction (RHEED) system.

SAW delay line devices were fabricated on the $AlN(0001)/Al_2O_3(11\bar{2}0)$ structures by a photolithography lift-off process. Aluminum with a thickness of ∼120 nm was deposited as unapodized IDT electrodes by an e-beam evaporation system. The SAW wavelength λ, which is twice the period of the IDT fingers, varies from 8 to 32 μm. Each device consists of two identical IDTs, with 50 pairs of fingers. The IDT center spacing, acoustic aperture, and finger width to space ratio are 120λ, 50λ, and 1 : 1, respectively.

In order to measure SAW characteristics as a function of the propagation angle, SAW devices at different wavelengths were patterned in groups inclined at a 15° interval starting from the $[1\bar{1}00]$ azimuth of $Al_2O_3(11\bar{2}0)$. We obtained the device frequency response and admittance by transmission and reflection coefficients measurements using a network analyzer. Important parameters for the design of an AlN based SAW device, such as $v_p$, $K^2$, and TCF, are derived based on the measurements.

## 3 Results and discussion

### 3.1 *Characterization of the AlN films*

A typical XRD scan of the $AlN(0001)/Al_2O_3(11\bar{2}0)$ structure is shown in Fig. 1 with a film thickness of 2 μm. The scan data feature a prominent AlN(0002) peak and a higher order AlN(0004) peak, along with a clean background free of other AlN orientations and impurities. As a result, our AlN films are fully *c*-plane oriented epitaxial films.

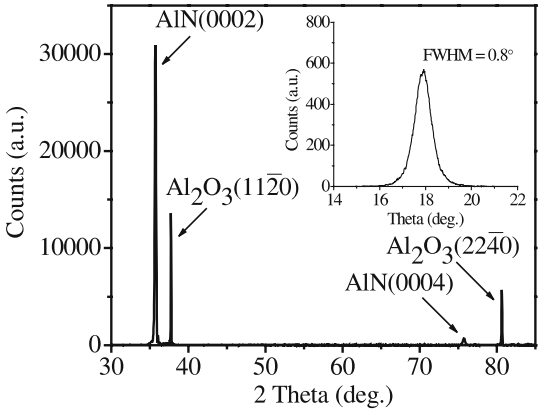


**FIGURE 1** XRD scan of the $AlN(0001)/Al_2O_3(11\bar{2}0)$ structure (film thickness: 2 μm). *Inset* is the AlN(0002) rocking curve with a FWHM of 0.8°

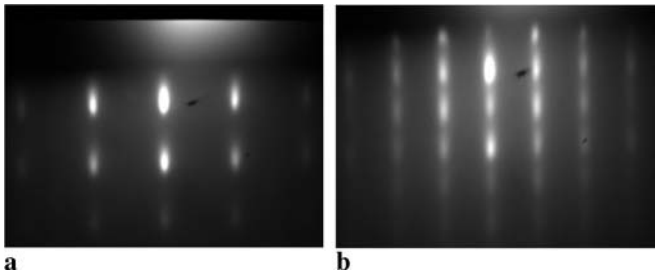


**FIGURE 2** RHEED patterns of the $AlN(0001)/Al_2O_3(11\bar{2}0)$ structure. The electron beam is incident in the (**a**) $Al_2O_3[0001]$ azimuth, (**b**) $Al_2O_3[1\bar{1}00]$ azimuth

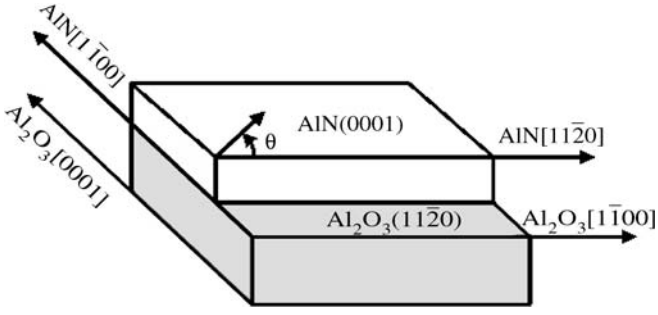


**FIGURE 3** Epitaxial growth relationships of the $AlN(0001)/Al_2O_3(11\bar{2}0)$ structure. The angle $\theta$ represents the SAW propagation angle measured from the $Al_2O_3[1\bar{1}00]$ reference

The full width at half maximum (FWHM) of the AlN(0002) rocking curves varies from 0.76° to 0.92° as the film thickness decreases, which indicates improved crystalline orientation as the film thickness increases. While the $Al_2O_3(11\bar{2}0)$ peak in Fig. 1 is well matched to its standard diffraction angle at 37.767°, a shift of −0.31° in the measured AlN(0002) peak from its power standard at 36.04° gives the estimation of the lattice constant *c* as 5.02 Å, slightly larger than the standard value of 4.979 Å [16]. The elongated *c* suggests a compressive strain field exists at the film substrate interface. This agrees with the reported work that the lattice mismatch of a $AlN(0001)/Al_2O_3(11\bar{2}0)$ structure along $Al_2O_3[0001]$ is 24.5%, higher than 13.3% in a $AlN(0001)/Al_2O_3(0001)$ structure [17].

The in situ RHEED pattern in Fig. 2a was taken when the electron beam incidents in the $Al_2O_3[0001]$ azimuth and it matches the theoretical pattern as an electron beam incidents in $[1\bar{1}00]$ azimuth of a (0001) wurtzite crystal; by rotating the substrate 90° around the substrate normal, the electron beam incidents in the $Al_2O_3[1\bar{1}00]$ azimuth and the resulting pattern in Fig. 2b conforms to that when the electron beam incidents in the $[11\bar{2}0]$ azimuth of a (0001) wurtzite crystal [18]. The epitaxial relationships of the $AlN(0001)/Al_2O_3(11\bar{2}0)$ structure are thus derived as $AlN[1\bar{1}00]//Al_2O_3[0001]$ and $AlN[11\bar{2}0]//Al_2O_3[1\bar{1}00]$ as illustrated in Fig. 3. A six fold symmetry of the AlN(0001) is also confirmed by the repeatability of the RHEED pattern when the substrate is rotated every 60° around its normal.

### 3.2 *Investigation on the SAW characteristics*

The $AlN(0001)/Al_2O_3(11\bar{2}0)$ structure studied here is a trigonal *YZ* plane overlaid by a *c*-plane hexagonal

thin film. Since the thin film thickness is usually less than the SAW wavelength, the anisotropic nature of the $Al_2O_3(11\bar{2}0)$ substrate is anticipated to induce deviations from otherwise isotropic behavior of the SAW propagation in an ideal semi-infinite hexagonal *c*-plane medium [19]. We choose here $Al_2O_3[1\bar{1}00]$ (AlN[$11\bar{2}0$]) as the 0° reference and all propagation angles, denoted as $\theta$ in Fig. 3, are measured counterclockwise to $Al_2O_3[1\bar{1}00]$ in a 180° semicircle.

The frequency responses of the devices at all angles were measured. Due to resemblance of the patterns, we only show typical responses for the devices propagating at 150° with three different wavelengths in the upper panel of Fig. 4. As the propagation angle varies, an additional higher velocity mode with smaller amplitude is found to coexist with the SAW, but only at 0°, 105°, and 180° off the reference $Al_2O_3[1\bar{1}00]$ (AlN[$11\bar{2}0$]). The lower panel of Fig. 4 demonstrated the corresponding frequency responses of such dual mode devices with a 0° propagation angle. Time domain gating technique is utilized in Fig. 4 to eliminate electromagnetic feed through and triple transit interference from the SAW signal to make the modes more discernable. The center frequency of the 2nd mode is ~ 1.05 times that of the coexisting SAW mode.

Figure 5 shows the angular dispersion of the $v_p$ of the SAW at different normalized film thicknesses, $kh = 0.4$, 0.9, and 1.7, where $k = 2\pi/\lambda$ and $h$ is the film thickness. The $v_p$ is calculated by multiplying peak frequency $f_0$ determined in the gated SAW frequency response by $\lambda$. Each data point in Fig. 5 represents an average velocity of multiple SAW devices with an error margin of a few m/s, much smaller than the velocity variation induced by angular changes. Compared to the SAW propagating in an AlN(0001)/$Al_2O_3$(0001) structure [2, 13], a more distinct angular dispersion ($v_p$ varying from 5503 to 6045 m/s) is observed with a two fold symmetry. The demonstrated angular dispersion gradually declines as $kh$ increases from 0.4 to 1.7, which indicates that the SAW propagation would asymptotically approach its isotropic nature in the hexagonal *c*-plane AlN as $h \gg \lambda$. Unlike the SAW mode, the $v_p$ of the higher frequency 2nd mode remains fairly constant along the excitation angle of 0°, 105°, and 180° at a fixed $kh$ value.

The angular dependence of $K^2$ of the SAW was investigated by means of IDT admittance measurements. By adopting a well known equivalent circuit model for IDTs [20, 21], the $K^2$ can be estimated as

$$K^2 = \frac{G_a(f_0)}{8 f_0 C_t N}, \tag{1}$$

where $G_a(f_0)$ is the IDT conductance measured at the resonance frequency, $N$ is the number of finger pairs per IDT port, and $C_t$ the total IDT capacitance defined as $C_t = NwC_s$ with $w$ the IDT acoustic aperture and $C_s$ the IDT static capacitance per finger pair per unit length. Here we take into account the parasitic contact resistance by finding the constant offset in the real part of the input impedance $Z$ and eliminate this value from the IDT admittance calculation [21]. The obtained $K^2$ values for different propagation angles are plotted in Fig. 6 for $kh = 0.4$, 0.9, and 1.7. They demonstrate distinctive angular dependence along with a trend of monotonous increase with respect to $kh$. The absolute values are in good agreement with those reported for AlN(0001) films [13, 22].

In Fig. 7, we plot $v_p$ as a function of $kh$ for both modes. For the SAW mode, the waves propagating along 150° and 60° define the upper and lower boundary of its velocity dispersion, respectively. The 15° propagating SAW is almost dispersionless, which could be advantageous for accurate frequency control in SAW applications regardless of the film thickness.

Phase velocity of the 2nd mode, as shown in Fig. 7, increases monotonically with the $kh$. To gain insight into this mode, comparisons between shear bulk wave velocities of the film and substrate are necessary as the mismatch between these velocities determines the type of acoustic mode that could be excited in the system. We calculate the shear vertical (SV) and SH bulk wave velocities ($v_{SV}$ and $v_{SH}$, re-

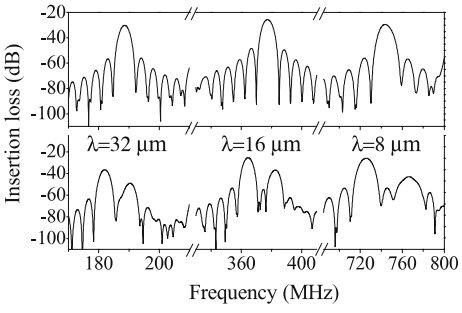


**FIGURE 4** The frequency response of the devices at different wavelengths. The *upper panel* is for the SAW devices propagating at 150°; the *lower panel* is for the SAW devices propagating at 0°

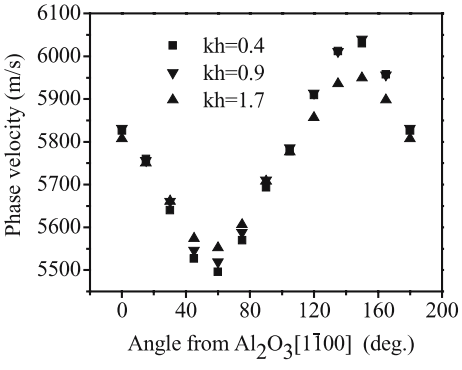


**FIGURE 5** Phase velocities of the SAW as a function of the propagation angle

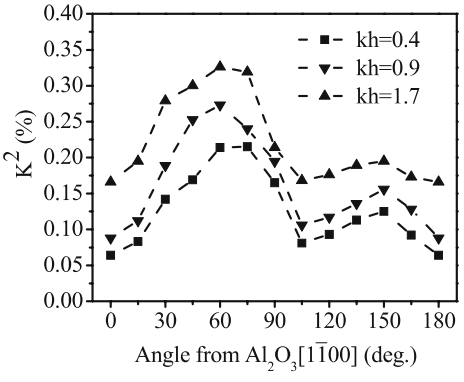


**FIGURE 6** Electromechanical coupling coefficients of the SAW as a function of the propagation angle

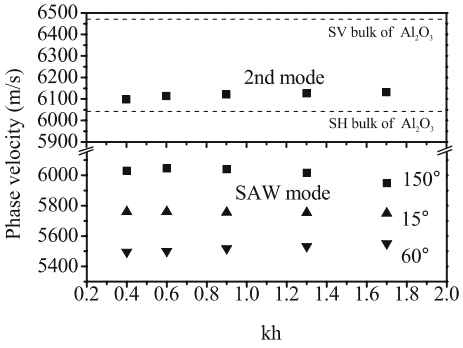


**FIGURE 7** Phase velocities as a function of the normalized film thickness $kh$. The *dotted lines* from the *bottom* to *top* represent $v_{SH}$ and $v_{SV}$ of $Al_2O_3(11\bar{2}0)$ at 0° propagation angle, respectively

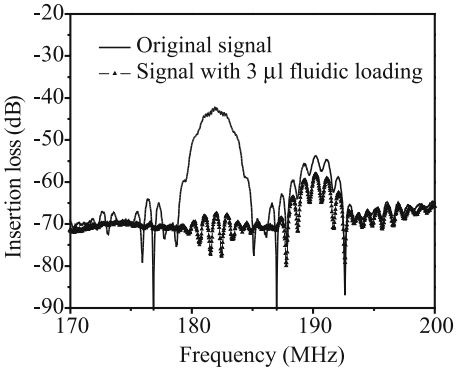


**FIGURE 8** Damping of the SAW and SH mode under liquid loading at wavelength $\lambda = 32\,\mu m$

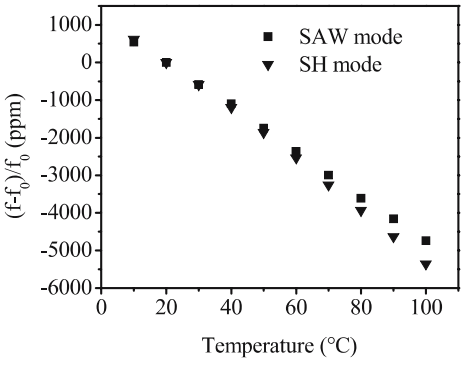


**FIGURE 9** Fractional frequency change as a function of temperature for the SAW and SH mode at a normalized film thickness of $kh = 0.4$

spectively) along the 0° reference for both AlN(0001) and $Al_2O_3(11\bar{2}0)$ based on the reported elastic constants [23, 24]. For AlN(0001), $v_{SV}$ is ∼6221 m/s, smaller than that of $Al_2O_3(11\bar{2}0)$ at ∼ 6473 m/s. Such a slow film/fast substrate system is known to support higher order overtones of Rayleigh SAWs when the film thickness goes beyond the SAW wavelength [6], a condition not created here. The existing boundary condition – a 6 mm class with basal axis normal to the plane also rules out the Bleustein–Gulyaev wave [25]. We further preclude the Love wave excitation as $v_{SH}$ of AlN(0001) at ∼ 6368 m/s is larger than that of $Al_2O_3(11\bar{2}0)$ at ∼ 6042 m/s. The leaky nature of the 2nd mode is demonstrated in Fig. 7 as the $v_p$ of the 2nd mode falls in between the slow $v_{SH}$ and fast $v_{SV}$ (dotted lines) of the $Al_2O_3(11\bar{2}0)$ at the same propagation angle. This indicates that the 2nd mode has a radiating SH partial mode into the $Al_2O_3(11\bar{2}0)$ substrate. We carried out a liquid damping experiment to further study the nature of the mode. In Fig. 8, we compare the frequency response of such a device before and after a 3 µl fluid loading in between IDTs. The ungated frequency response is displayed for accurate determination of the insertion loss. A strong damping of 25 dB is observed on the SAW mode as opposed to only 4 dB on the 2nd mode. This confirms a large SH particle displacement in the 2nd mode. Considering the specific excitation angles and SH polarization, the higher velocity 2nd mode is believed to be a PSAW which arises from the acoustic bulk phonons' contribution in anisotropic media, and happens to have sharp resonances at the observed angles [19].

The fractional change in device resonance frequency as a function of temperature is shown in Fig. 9, where $f_0$ is selected as the resonance frequency at 20 °C. Both modes show a linear decrease in their resonance frequencies with increasing temperature over the range we consider. The TCF is determined from the following equation:

$$\mathrm{TCF} = \frac{1}{f_0} \times \frac{\mathrm{d}f}{\mathrm{d}T}\,. \tag{2}$$

The calculated TCF from the least-square fit of the data are −59 and −63 ppm/°C for the SAW and SH mode ($kh = 0.4$), respectively. Such values fall into the range of those reported for the SAW devices on AlN thin film structures, which extend from −80 to 20 ppm/°C [7, 13, 14]. The increment in $kh$ only has a minor effect (∼7% reduction in TCF) on the TCF for both modes. Nevertheless, the near linear relationship between the resonance frequency and temperature would be advantageous to develop temperature compensation algorithms for real applications.

## 4 Conclusions

AlN thin films were epitaxially deposited on $Al_2O_3(11\bar{2}0)$ substrates with orientation relationships given as AlN(0001)/$Al_2O_3(11\bar{2}0)$ and AlN$[1\bar{1}00]$//$Al_2O_3$ [0001]. We studied the SAW characteristics in such structures with respect to the propagation angles and normalized film thicknesses. It is noteworthy that a higher velocity SH mode is found to coexist with the SAW at 0°, 105°, and 180° off the reference $Al_2O_3[1\bar{1}00]$, over the respective angular period. The measured phased velocity and electromechanical coupling coefficient of the SAW show strong anisotropic effects associated with the anisotropic $Al_2O_3(11\bar{2}0)$ substrate. The SH mode has the characteristics of a PSAW excited at isolated crystal angles. The strong SH polarization in this mode makes it promising for liquid based biosensing applications.

**ACKNOWLEDGEMENTS** This work was supported in part by NIH grant 1RO1EB00741-01, DoD grant DAAE07-03-C-L140, and the Smart Sensors and Integrated Microsystems program at Wayne State University.

## REFERENCES

1 C. Deger, E. Born, H. Angerer, O. Ambacher, M. Stutzmann, J. Hornsteiner, E. Riha, G. Fischerauer, Appl. Phys. Lett. **72**, 2400 (1998)
2 H. Okano, N. Tanaka, Y. Takahashi, T. Tanaka, K. Shibata, S. Nakano, Appl. Phys. Lett. **64**, 166 (1994)

3 D.S. Ballantine, R.M. White, S.J. Marti, A.J. Ricco, E.T. Zeller, G.C. Frye, H. Wohltjen, *Acoustic Wave Sensors: Theory, Design, and Physico-Chemical Applications* (Academic, NY, 1997)
4 M.J. Vellekoop, Ultrasonics **36**, 7 (1998)
5 J. Xu, G. Hu, G.W. Auner, H. Ying, Electron. Lett. **41**, 1254 (2005)
6 Y. Takagaki, P.V. Santos, E. Wiebicke, O. Brandt, H.P. Schonherr, K.H. Ploog, Phys. Rev. B **66**, 1 (2002)
7 O. Elmazria, V. Mortet, M. Hakiki, M. Nesladek, P. Alnot, IEEE Trans. Ultrason. Ferroelectr. Freq. Control **50**, 710 (2003)
8 K.S. Kao, C.C. Cheng, Y.C. Chen, Y.H. Lee, Appl. Phys. A **76**, 1125 (2003)
9 T.C. Lim, W. Farnell, J. Acoust. Soc. Am. **45**, 845 (1969)
10 I.S. Didenko, F.S. Hickernell, N.F. Naumenko, IEEE Trans. Ultrason. Ferroelectr. Freq. Control **47**, 179 (2000)
11 M. Lewis, IEEE Ultrason. Symp. Proc. **2**, 744 (1977)
12 N.F. Naumenko, I.S. Didenko, Appl. Phys. Lett. **75**, 3029 (1999)
13 K. Tsubouchi, N. Mikoshiba, IEEE Trans. Sonics Ultrason. **SU-32**, 634 (1985)
14 K. Kaya, Y. Kanno, H. Takahashi, Y. Shibata, T. Hirai, Jpn. Appl. Phys. **35**, 2782 (1996)
15 P.K. Guo, G.W. Auner, Z.L. Wu, Thin Solid Films **253**, 223 (1994)
16 K. Dovidenko, S. Oktyabrsky, J. Narayan, J. Appl. Phys. **79**, 2439 (1996)
17 C.J. Sun, P. Kung, A. Saxler, H. Ohsato, K. Harita, M. Razeghi, J. Appl. Phys. **75**, 3964 (1994)
18 H. Okano, N. Tanaka, M. Kobayashi, T. Usuki, K. Shibata, Jpn. J. Appl. Phys. **34**, 5172 (1995)
19 G.W. Farnell, *Physical Acoustics VI* (Academic, NY, 1970)
20 C. Campbell, *Surface Acoustic Wave Devices and Their Signal Processing Applications* (Academic, NY, 1989)
21 J.H. Hines, D.C. Malocha, IEEE Ultrason. Symp. Proc. **1**, 173 (1993)
22 C. Caliendo, Appl. Phys. Lett. **83**, 4853 (2003)
23 L.E. McNeil, M. Grimsditch, R.H. French, J. Am. Ceram. Soc. **76**, 1132 (1993)
24 E. Dieulesaint, D. Royer, *Elastic Waves in Solid* (Wiley, Chichester, 1990)
25 J.L. Bleustein, Appl. Phys. Lett. **13**, 412 (1968)